Use of Training Subcarriers for Synchronization in Low Latency Uplink Communication with GFDM

Kiwon Lee*, Mingeun Kang*, Eui-Rim Jeong†, Dong-Jo Park*, and Yong H. Lee*
*School of Electrical Engineering, Korea Advanced Institute of Sceience and Technology (KAIST), Daejeon, Korea
†Dept. of Information and Communication Engineering, Hanbat National University, Daejeon, Korea
Email: {kaiser5072, minkang}@stein.kaist.ac.kr ,erjeong@hanbat.ac.kr, {djpark, yohlee}@kaist.ac.kr

***Abstract*—We consider low latency uplink communication where users transmit their signal using generalized frequency division multiplexing (GFDM) with K subcarriers and M subsymbols. The proposed approach for synchronization exploits both training subcarriers and training subsymbols *embedded* in a GFDM symbol. A frequency domain training sequence (FD-TS) of length M is loaded on each training subcarrier, and at the receiver the corresponding time domain TS (TD-TS) of length $N = KM$ is extracted by filtering the received signal. We employ FD-TSs having two identical halves of length $M/2$ so that the corresponding TD-TS has two identical halves of length $N/2$. The extracted TD-TS is used for coarse timing synchronization and carrier frequency offset (CFO) estimation. The training subsymbol of the proposed scheme is used only for fine timing synchronization. The synchronization approach with the proposed training structure is compared with the existing method exploiting only training subsymbols. The results demonstrate that the former outperforms the latter in CFO estimation, while requiring less TS overhead; both the approaches perform well in acquiring timing synchronization.**

***Index Terms*—low latency, GFDM, single-shot transmission, synchronization, embedded training sequence.**

I. Introduction

GFDM has been proposed as a useful extension of popular orthogonal frequency division multiplexing (OFDM) [1]. In GFDM, a symbol is composed of multiple subcarriers and multiple subsymbols, where the input data loaded on each subcarrier is oversampled and pre-filtered (or pulse shaped) through a circular convolution between the oversampled input and filter coefficients. GFDM transmitting N samples using K subcarriers and M subsymbols, where $N = KM$, reduces to OFDM with N subcarriers if $M = 1$ and to single-carrier frequency division multiplexing (SC-FDM) if the pulse shaping process is dropped. By employing a proper pulse shaping filter (PSF), GFDM can reduce the out of band (OOB) emissions and peak to average power ratio (PAPR) [2]. Due to its flexible architecture and capability in reducing OOB emissions and PAPR, GFDM would be a useful alternative to OFDM in the next generation mobile communications, where opportunistic/dynamic spectrum access and transmission with low power consumption are required for applications such as machine-to-machine (M2M) communication [3] and Tactile Internet [4].

One of the key features needed for Tactile Internet and vehicle-to-vehicle (V2V) [5] applications are the low latency communication which demands the use of short bursts of data. If GFDM is employed in such systems, each data burst (or frame) consists of only a few GFDM symbols, meaning that minimizing the overhead of training sequences (TSs), pilots and cyclic prefix (CP) is essential. This issue has been addressed in [6], [7]. In these works the authors propose the use of two identical training subsymbols: in [6] an isolated training structure that separates the training and data subsymbols by a CP is proposed, while in [7] an embedded training structure that places training subsymbols in the center of the GFDM symbol is proposed. The latter needs less overhead than the former, but its performance in estimating the CFO is degraded by the interference from the data subsymbols.

In this paper, we propose another type of embedded TS for low latency uplink communication, where each user aligns its transmit signal to the reference signal from the base station (BS) and sends one GFDM symbol at each transmission (single-shot transmission [7]). In contrast to the *embedded midamble* (EM) in [7] consisting of only training subsymbols, the proposed TS is a hybrid of a training subsymbol and training subcarriers. In the proposed training structure, called the *hybrid training* (HT) structure, FD-TSs of span M are loaded on the training subcarriers and at the receiver the corresponding TD-TS of span $N = KM$ is extracted by filtering the received signal. We employ FD-TSs having two identical halves of length $M/2$ so that the corresponding TD-TS has two identical halves of length $N/2$. The extracted TD-TS is used for coarse timing synchronization and CFO estimation. For fine timing acquisition we employ one training subsymbol. The performances of synchronization using the proposed HT and the existing EM are compared through computer simulation. The results indicate that the proposed scheme performs well in the uplink scenario, where the symbol timing offset (STO) is upper-bounded by the channel delay spread (CDS) and propagation delay, and outperforms the existing scheme in CFO estimation, while requiring less TS overhead; both the methods work well for timing synchronization.

The organization of this paper is as follows. In Section II, we review the GFDM transmitter and describe the communication scenario. Section III states the HT design and analyzes the au-

This work was supported by ICT R&D program of MSIP/IITP. B0101-16-1369, Development of small basestation supporting multiple streams based on LTE-A systems

tocorrelation property. Section IV presents the synchronization method for HT. The simulation results are provided in Section V, and finally the conclusion is described in Section VI.

II. System Model

A. GFDM Transmitter

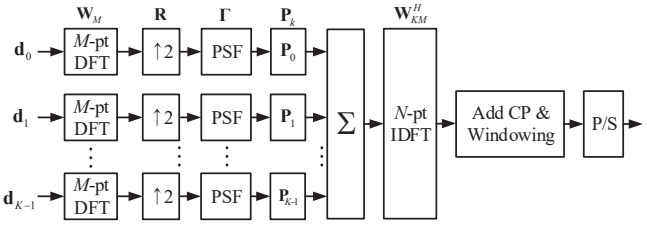

Fig. 1. Structure of a GFDM transmitter.

Consider a system transmitting GFDM symbols with K subcarriers and M subsymbols. Each GFDM symbol carries N input samples where $N = KM$. The input samples are partitioned into M-dimensional disjoint vectors, denoted as $\mathbf{d}_k$ for $k = 0, 1, , K-1$. Then each vector $\mathbf{d}_k$ is passed through the branch consisting of the M-point DFT, L-fold upsampler, and pulse shaping filter (PSF) blocks, where we set $L = 2$ (Fig. 1). The outputs from the branches are added, and then the N-point inverse DFT (IDFT) is performed to yield the N-dimensional transmit vector $\mathbf{x}$. Finally, the CP is added to $\mathbf{x}$ before transmission. To be specific, let the transmit vector be written as [2]

$$\mathbf{x} = \mathbf{W}_N^H \sum_{k=0}^{K-1} \mathbf{P}_k \mathbf{\Gamma} \mathbf{R} \mathbf{W}_M \mathbf{d}_k, \tag{1}$$

where $\mathbf{W}_M$ and $\mathbf{W}_N^H$ are the M-point DFT and N-point IDFT matrices; $\mathbf{R}$ is the $2M \times M$ upsampling matrix given by $\mathbf{R} = [\mathbf{I}_M \ \mathbf{I}_M]^T$ for $\mathbf{I}_M$ denoting the M dimensional identity matrix; $\mathbf{\Gamma}$ is a $2M \times 2M$ diagonal matrix whose diagonal entries are given by the $2M$-point DFT of the PSF's impulse response; and $\mathbf{P}_k$ is a $KM \times LM$ matrix that maps $\mathbf{d}_k$ to the k-th subcarrier. $\mathbf{P}_k$ is a block matrix consisting of 2 identity matrices $\mathbf{I}_M$ and $(K-2)$ all-zero $M \times M$ matrices 0_M, as shown below.

$$\mathbf{P}_0 = \left[\begin{array}{c|ccc} \mathbf{I}_M & \overbrace{\mathbf{0}_M & \cdots & \mathbf{0}_M}^{K-1} \\ \underbrace{\mathbf{0}_M & \cdots & \mathbf{0}_M}_{K-1} & \mathbf{I}_M \end{array} \right]^T$$

$$\mathbf{P}_k = \left[\begin{array}{ccc|ccc} \overbrace{\mathbf{0}_M & \cdots & }^{k} & \mathbf{0}_M & \mathbf{I}_M & \overbrace{\mathbf{0}_M & \cdots & \mathbf{0}_M}^{K-k-1} \\ \underbrace{\mathbf{0}_M & \cdots & \mathbf{0}_M}_{k-1} & \mathbf{I}_M & \underbrace{\mathbf{0}_M & \cdots & \mathbf{0}_M}_{K-k} \end{array} \right]^T$$

for $1 \le k \le K-1$.

B. Communication scenario

In the uplink communication scenario considered in this paper, the users transmit their GFDM symbols if the channel appears empty, obeying a carrier sensing multiple access (CSMA) protocol, and at each transmission they send only one GFDM symbol (single-shot transmission). The base station periodically transmits its reference signal with period T_B; each user aligns its uplink signal to the BS time and frequency by exploiting the reference signal. As a result, the user sends the signal at time $t = iT_B + \tau_p$ and frequency $f_c + \Delta f$, where i is a non-negative integer determined by carrier sensing, τ_p is the propagation delay; f_c is the carrier frequency, and Δf is the CFO due to Doppler shift and the residual frequency offset. It is assumed that collision does not occur, and the base station receives the signal at time $iT_B + 2\tau_p$ and frequency $f_c + \Delta f$. Under this scenario, the network becomes perfectly time-synchronized if the CP length accommodates both the CDS and the two-way propagation delay ($2\tau_p$) [8]. This is an attractive feature, but requires increasing the CP length by $2\tau_p$, as compared with a common CP that accommodates only the CDS. To reduce latency, we employ a shorter CP and perform timing synchronization at the base station. In this uplink scenario the symbol timing offset (STO), denoted as n_0, is limited in the range

$$0 \le n_0 \le N_{cds} + 2N_p \tag{2}$$

where the time index 0 represents the time iT_B, $N_{cds} = \lceil \frac{\tau_{cds}}{T_S} \rceil$, and $N_p = \lceil \frac{\tau_p}{T_s} \rceil$ for T_s denoting the sampling period.

III. Training Structures

We use two sets of subcarriers for training where each set contains K_T successive subcarriers ($K_T << K$). To achieve frequency diversity, one set is located in the lowest frequencies and the other is located in the highest frequencies of the GFDM symbol. Since the two sets are symmetric in the frequency domain, a high-pass filter with real-valued impulse response can be used for extracting the TD-TS at the receiver. A guard band consisting of K_{GB} successive subcarriers is placed in between the sets of training and data subcarriers ($K_{GB} << K$). The proposed training and guard subcarriers can be fitted into a GFDM symbol, as shown in the following example:

Example 1. Let $K_T = 2$, $K_{GB} = 1$. Assuming that the total number of subcarriers K is an even number, the training subcarriers are located at $\{K/2, K/2+1, K/2-2, K/2-1\}$ subcarrier positions where the first (last) two correspond to the lowest (highest) frequencies. The guard bands are placed at $\{K/2+2, K/2-3\}$.

This type of TS structure placing $2K_T$ training subcarriers and $2K_{GB}$ guard subcarriers in a GFDM symbol will be referred to as the *embedded training subcarrier* (ET-SC) structure. To compare the ET-SC with the EM, the GFDM input vectors $\{d_0, \ldots, d_{K-1}\}$ are arranged as a $K \times M$ matrix whose k-th row is given by $\mathbf{d}_{k-1}^T$. In the case of EM, two sample positions in the middle of each $\mathbf{d}_k$ are filled with two identical pilot samples, denoted as $\mathbf{c}_k$ (Fig. 2a). This pilot insertion results in two training subsymbols located in the middle of the GFDM symbol. A pseudonoise (PN) sequence can be used for $\{c_o, \ldots, c_{K-1}\}$. On the other hand, the ET-SC allocates an M-dimensional training vector to each training

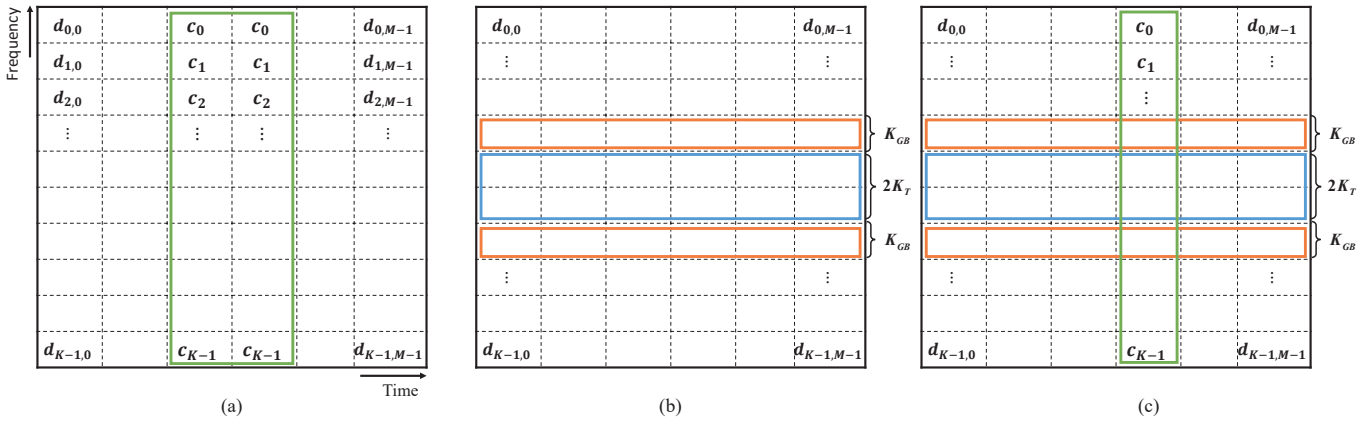

Fig. 2. A GFDM symbol with embedded training sequence. (a) Embedded Midamble. (b) Embedded Training Subcarrier. (c) Hybrid Training.

subcarrier (Fig. 2b). The training vector for the k-th training subcarrier is denoted as $\mathbf{p}_k$. We use $\mathbf{p}_k$ with two identical halves of length $M/2$ so that the extracted TD-TS at the receiver exhibits two repeated parts in the ideal, noise-free case. The proposed HT structure is a hybrid of ET-SC and EM (Fig. 2c). For the EM part of HT, we allocate only one pilot sample to each subcarrier, because this part is exploited only for fine timing acquisition. Due to the fact that the HT structure needs only one training subsymbol, the training overhead of HT can be considerably less than that of EM.

Next we examine the autocorrelation characteristics of the TD-TS in the N-dimensional transmit vector $\mathbf{x}$ in (1). Let $\mathbf{v}_{EM}, \mathbf{v}_{ET}$, and $\mathbf{v}_{HT}$ denote the training parts of the $\mathbf{x}$ vectors corresponding to the EM, ET-SC and HT, respectively. These training vectors can be obtained by using PN training sequences in the structures of Fig. 2, while setting the data samples $\{d_{k,m}\}$ at zero. The vector $\mathbf{v}_{HT}$ can be written as

$$\mathbf{v}_{HT} = \mathbf{v}_{ET} + \mathbf{v}_{HT-M} \tag{3}$$

where $\mathbf{v}_{HT-M}$ is the N-dimensional training vector corresponding to the EM part of HT. We denote the TD-TSs corresponding the training vectors by $\{v_{EM}[n]\}$, $\{v_{ET}[n]\}$, and $\{v_{HT}[n]\}$, which are equal to $\mathbf{v}_{EM}$, $\mathbf{v}_{ET}$, and $\mathbf{v}_{HT}$, respectively, if $0 \le n \le N-1$, and zero, otherwise. Note that $\{v_{ET}[n] \mid 0 \le n \le N-1\}$ has two identical halves of span $N/2$. For $v_{EM}[n]$, the normalized autocorrelation is written as

$$c_{EM}[n] = \frac{\sum_{j=0}^{N-1} v_{EM}^*[n+j]v_{EM}[j]}{\sum_{j=0}^{N-1} v_{EM}^*[j]v_{EM}[j]} \tag{4}$$

Likewise, the normalized autocorrelations for the other TD-TSs can be written. Fig. 3 shows the normalized autocorrelations when binary PN sequences are employed. As expected, the autocorrelations of the EM and the EM part of HT ($\mathbf{v}_{HT-M}$ in (3)) overlap and exhibit sharp trajectory. On the other hand, those of ET-SC and HT exhibit multiple peaks with degraded sharpness. This occurs because of the K-fold interpolation involved in converting the M-dimensional FD training vectors in the training subcarriers into the N-dimensional TD vector $\mathbf{v}_{ET}$. This autocorrelation characteristic of ET-SC limits the use of the ET-SC part of HT to coarse timing acquisition of uplink signals where the STO is bounded by (2).

Although $\{v_{ET}[n]\}$ does not exhibit desirable autocorrelation properties, it has two identical halves of length $N/2$, because each training vector $\mathbf{p}_k$ of ET-SC has two identical halves of length $M/2$. We exploit this repetitive structure for coarse timing synchronization and CFO estimation.

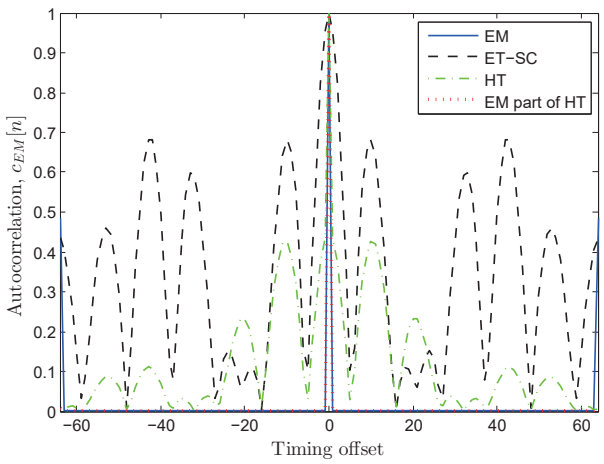

Fig. 3. Normalized autocorrelations.

IV. Synchronization Methods

The proposed synchronization process is illustrated in Fig.4. The received signal $r[n]$ is passed through a high-pass filter, to extract the TD-TS which corresponds to the ET-SC part of HT, $\{v_{ET}[n] \mid 0 \le n \le N-1\}$, having two identical halves of length $N/2$. The extracted TD-TS, denoted as $r_f[n]$, is used for both coarse timing sync and CFO estimation. The two halves of $\{v_{ET}[n] \mid 0 \le n \le N-1\}$ will remain identical after passing through the channel and the high-pass filter

except for a phase shift induced by the CFO. Thus, ignoring noise, $r_f[n]$ can be written as [8],

$$r_f[n] = s[n] \cdot e^{j2\pi\epsilon n/K}, \tag{5}$$

and

$$r_f[n + N/2] = s[n] \cdot e^{j2\pi\epsilon n/K} \cdot e^{j\pi\epsilon M}, \tag{6}$$

where $0 \leq n \leq N_{cds} + 2N_p$ (see (2)); $s[n]$ represents the useful signal; and ϵ is the CFO normalized to the sub-carrier spacing $1/KT_s$ for T_s denoting the sampling period ($\epsilon = KT_s\Delta f$). We see from (6) that $|\epsilon| \leq 1/M$, and the proposed scheme functions when the CFO is bounded as

$$|\Delta f| \leq 1/(NT_s). \tag{7}$$

The coarse timing acquisition and CFO estimation can be performed by applying a sliding window correlator of lag $N/2$ to $r_f[n]$. The estimates of coarse STO and CFO, denoted as $\hat{n}_c$ and $\hat{\epsilon}$, respectively, are written as [8], [9].

$$\hat{n}_c = \arg\max_n \{|c_r[n]|\}, \tag{8}$$

and

$$\hat{\epsilon} = \frac{1}{M\pi} \arg\{c_r[\hat{n}_c]\}, \tag{9}$$

where $c_r[n]$ is the normalized autocorrelation function:

$$c_r[n] = \frac{\sum_{j=0}^{N-1} r_f^*[j+n] r_f[j+n+N/2]}{\sum_{j=0}^{N-1} r_f^*[j] r_f[j+N/2]}, \tag{10}$$

for $0 \leq n \leq N_{cds} + 2N_p$.

Again referring to Fig. 4, we evaluate $r'[n]$ which is the difference between $r[n]$ and $r_f[n]$ to remove the ET-SC part from the received signal, and then the CFO is compensated by multiplying $e^{j\frac{2\pi\hat{\epsilon}n}{K}}$ with $r'[n]$. Finally, the fine timing acquisition is achieved by cross-correlating the output of CFO compensator with $v_{HT-M}[n]$ which is a TD-TS corresponding to the EM part of HT (see (3)).

In the proposed scheme, the result of coarse timing sync is used only for CFO estimation. In the uplink scenario, the residual STO after coarse timing sync is upper-bounded by $N_{cds} + 2N_p$ (see (2)). In what follows, we shall show through computer simulation that the CFO estimator in (9) is robust to the STO estimation error when $N_{cds} + 2N_p$ is less than 25% of the symbol duration N.

V. Simulation Results

The synchronization performance of the proposed scheme with HT structure is compared with those of the ET-SC, isolated preamble [6] and EM [7] through computer simulation considering two types of channels, called the pedestrian and vehicular channels [10]. The GFDM system and channel parameters for the simulation are listed in Table I. Since $N = MK = 512$ and $1/T_s$ = 20 MHz, the CFO upper-bound $1/(NT_s)$ in (7) is about 39KHz, indicating that the proposed CFO estimator should function in the uplink scenario, because Doppler shift of practical systems such as LTE is typically less than 1 KHz. The GFDM assumes Dirichlet pulse shape, and

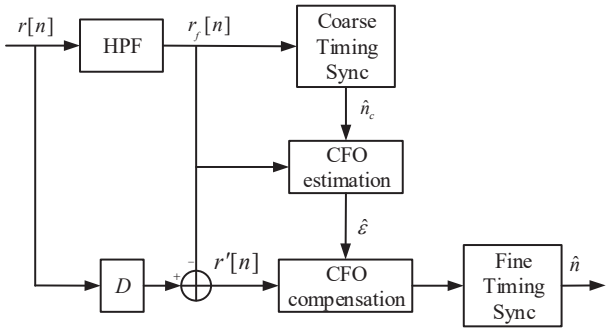

Fig. 4. Proposed synchronization process where *D* represents the delay which is equal to the group delay of the high-pass filter (HPF).

the duration of CP is set at N_{cds}: the CP duration is 8 and 50 for pedestrian and vehicular channels, respectively. The cell radius is 500 m, and the maximum propagation delay, N_p, is 32 samples ($\tau_p = 1.67\mu s$). Thus the upper-bound, $N_{cds}+2N_p$, of the search range for STO estimation is 72 and 114 for pedestrian and vehicular channels, respectively. Note that the search range is less than 25% of the symbol duration $N = 512$.

TABLE I
Simulation parameters

Parameters	**Values**
PSF	Dirichlet
Number of subcarriers (K)	64
Number of subsymbols (M)	8
CFO (ϵ)	0.01 (3.2 kHz)
Sampling frequency ($1/T_s$)	20 MHz
Propagation delay, N_p	32 samples
CP length=N_{cds}	Pedestrian: 8 samples Vehicular: 50 samples

The performance for timing synchronization is examined by evaluating the probability of false acquisition, P_{FA}, defined as

$$P_{FA} = 1 - \Pr[0 \leq \hat{n} - n_0 \leq N_{cds}]. \tag{11}$$

Here we declare that timing sync is acquired when the STO estimation error, $\hat{n} - n_0$ is in between 0 and N_{cds}. This can be justified, because the residual STO in this range can be compensated during FD channel equalization. The CFO estimation performance is examined by evaluating the mean square error (MSE) between $\hat{\epsilon}$ and ϵ. The P_{FA} and MSE are evaluated for 100,000 realizations at each value of the signal-to-noise ratio (SNR) with fixed STO and CFO: $n_0 = 36$ (pedestrian) and 57 (vehicular); $\epsilon = 0.01$. We use a 31-tap finite impulse response (FIR) high-pass filter for extracting the ET-SC part of HT.

Table II lists the P_{FA} values when the SNR is in between 5dB and 25dB. The P_{FA} values of the HT, EM and isolated preamble are less than 10^{-4} for all SNR values in the range; this holds true for both the pedestrian and vehicular channels. On the other hand, the P_{FA} values of ET-SC are about 10^{-1} for all SNR values of the two channels, indicating that the use of ET-SC needs some caution. In the proposed HT-based

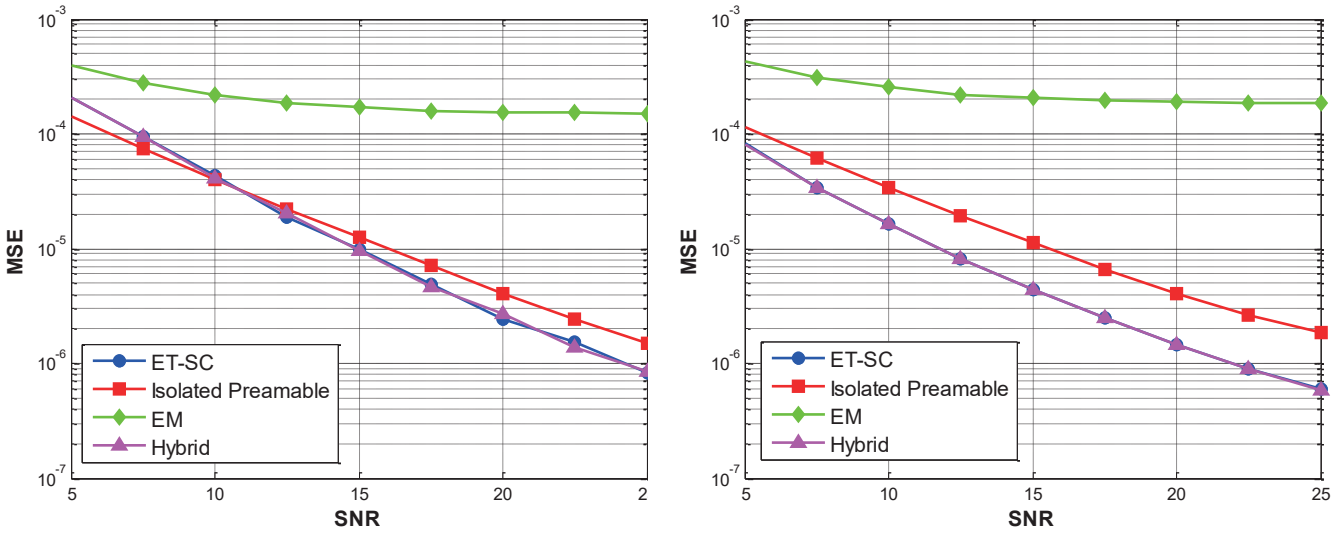

Fig. 5. MSEs of CFO estimator (a) Pedestrian channel. (b) Vehicular channel.

scheme, the coarse STO estimate obtained by exploiting the ET-SC part of HT, is not used for fine timing sync but used only for CFO estimation.

TABLE II
$\mathbf{P_{FA}}$ VALUES WHEN SNR IS IN BETWEEN 5dB AND 25dB.

	ET-SC	Isolated	EM	Proposed
Pedestrian and Vehicular	$\approx 10^{-1}$	below 10^{-4}	below 10^{-4}	below 10^{-4}

Fig. 5 shows the MSE of the CFO estimate against SNR. In CFO estimation, the EM performs the worst; and for most SNR values of the two channels, the ET-SC and HT perform better than the isolated preamble exploiting two identical subsymbols of length $K = 64$. This happens because the length of the TD-TSs for CFO estimation in the ET-SC and HT schemes is $N = 512$, while that of the isolated preamble is $2K = 128$. These results demonstrate that the CFO estimator of the proposed scheme is robust to the STO estimation error in this uplink setting, where $\tau_{cds} + 2\tau_p$ is less than 25% of the symbol duration N.

The training overheads of the HT and EM based schemes, exploiting embedded TSs, are 18% and 25%, respectively. The comparisons between the two embedded TSs lead to the following statement: the HT based scheme can outperform the EM based scheme in CFO estimation, while requiring less overhead; both the schemes perform well for timing synchronization.

VI. Conclusion

We proposed the HT embedded in a GFDM symbol as a useful alternative to the existing embedded training, called the EM. The HT exploits training subcarriers as well as training subsymbols, while the EM employs only training subsymbols. It is shown that the training subcarriers of HT are particularly useful for CFO estimation in an uplink scenario where the STO is upper-bounded by the CDS and the propagation delay, and the STO upper-bound is a fraction of the GFDM symbol duration. The simulation results demonstrate the advantage of the HT-based synchronization over the EM-based: the former can outperform the latter in CFO estimation, while requiring less overhead; both the schemes perform well for timing synchronization.

The EM part of HT can be used for channel estimation. Further works include channel estimation, equalization and bit error ratio (BER) analysis for GFDM systems with HT.

References

[1] N. Michailow, M. Matthé, I. S. Gaspar, A. N. Caldevilla, L. L. Mendes, A. Festag, and G. Fettweis, "Generalized frequency division multiplexing for 5th generation cellular networks," *IEEE Trans. Commun.,* vol. 62, no. 9, pp. 3045-3061, 2014.

[2] N. Michailow and G. Fettweis, "Low peak-to average power ratio for next generation cellular systems with genenralized frequency division multiplexing," in *Proc. Int. Symp. ISPACS,* Naha, Japan, pp. 651-655, Nov. 2013.

[3] Y. Ding, Y. Jin, L. Ren, and K. Hao, "An intelligent self-organization scheme for the Internet of things," *IEEE Comput. Intell. Mag.,* vol. 8, no. 3, pp. 41-53, Aug. 2013.

[4] G. Fettweis, "The tactile Internet: Applications and challenges," *IEEE Veh. Technol. Mag.,* vol. 9, no. 1, pp. 64-70, Mar. 2014.

[5] M. Nekovee, "Quantifying performance requirements of vehicle-to-vehicle communications protocols for rear-end collision avoidance," in *Proc. IEEE 69th Veh. Technol. Conf.,* Barcelona, vol. 1, pp. 1-5, Apr. 2009.

[6] I. S. Gaspar, L. L. Mendes, N. Michailow, and G. Fettweis, "A synchronization technique for generalized frequency division multiplexing," *EURASIP Journal on Advances in Signal Processing,* 2014.

[7] I. Gaspar, G. Fettweis, "An embedded midamble synchronization approach for generalized frequency division multiplexing," in *Proc. IEEE Global Commun. Conf.,* San Diego, CA, USA, Dec. 2015.

[8] M. Morelli, C. J. Kuo, and M. O. Pun, "Synchronization techniques for orthogonal frequency division multiple access (OFDMA): A tutorial review," *Proceedings of the IEEE*, vol. 95, no. 7, pp. 1394-1427, Jul. 2007.

[9] T. Schmidl and D. Cox, "Robust frequency and timing synchronization for OFDM," *IEEE Trans. Commun.,* vol. 45, no. 12, pp. 1613-1621, Dec. 1997.
[10] 3GPP, "Technical specification 36.104," Tech. Rep., Jan. 2016, v13.2.0.